Flip Bifurcation and Chaos in Three-State Boost Switching Regulators

C. K. Tse, *Member, IEEE*

Abstract— **A first-order iterative map that describes the dynamics of a simple feedback boost switching regulator operating in discontinuous mode is derived. Analysis of this map shows that flip bifurcations occur at certain values of the feedback factor. Results from computer simulations and experiments reveal that the system exhibits a typical period-doubling route to chaos under the particular operating condition studied in this paper. It is found that a special kind of randomness, arising from the ability of the system to change its configuration in more than one predefined patterns, constitutes a unique feature of the chaotic dynamics of switched-mode converter circuits.**

I. Introduction

CHAOTIC behavior is not at all uncommon in switching power supplies, despite the fact that its presence is often ignored by practical circuit designers [1],[2]. When the power supply engineer sees some unexpected behavior in his circuit, his usual reaction is to try to force the circuit back to its regular periodic state by adjusting certain components that he believes are causing trouble to his circuit. Investigation into the real cause of the problem does not seem to interest the engineer, whose major objective is to ensure that the circuit operates in its expected regular regime. On the contrary, system theorists and mathematicians, over the past two decades, have been actively investigating chaos and its underlying cause. Many theoretical and numerical results were generated that suggested plausible explanations to many strange phenomena observed in physical and hypothetical systems [3]–[5]. Our objectives in this paper are two-fold. To switching regulator practitioners, we try to explain some commonly seen, but often ignored, "strange" phenomena exhibited by switching regulators. To circuit and system theorists, we report chaotic behavior observed in a boost switching regulator. Although our focus in this paper is on one particular mode of operation of the boost regulator, our result regarding structural instability of the system holds for the general class of converter circuits.

We shall first derive a first-order iterative map that describes the open-loop dynamics of the system. Then, with the loop closed, the feedback factor becomes a parameter that can be varied at will. The resulting iterative map of the closed-loop system is of the form

$$x_{n+1} = f(x_n, \kappa) \tag{1}$$

Manuscript received January 9, 1992; revised June 22, 1993. This work was supported in part by the Hong Kong Polytechnic Research Sub-Committee under Grant 341.166.A3.420. This paper was recommended by Associate Editor Martin Hasler.

The author is with the Department of Electronic Engineering, Hong Kong Polytechnic, Hong Kong.

IEEE Log Number 9214334.

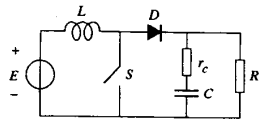

Fig. 1. Circuit diagram of the simple boost converter.

where x_n denotes the state at the nth switching instant and κ denotes the feedback factor.

The results of our investigation will be reported in three stages. First, based on (1), and using κ as the bifurcation parameter, the onset of flip bifurcation is located and a period-doubling route to chaos predicted. Second, computer simulation based on the *exact* state equations confirms the presence of the period-doubling sequence of subharmonic oscillations and the chaotic asymptotic behavior. Finally, a circuit is constructed to experimentally demonstrate the occurrence of subharmonics and chaos.

II. Exact State Equations

As is common to all power electronic systems, the switching regulator is a *multi-structural* system with its circuit topology varied according to the states of the switches. Fig. 1 shows the simple boost converter, with the equivalent-series-resistance r_c of the output capacitor included. Normally, the switch and the diode are turned on and off in a *complementary* fashion, i.e., one is on while the other is off, and vice versa. The inductance current, in this case, is always nonzero, and the circuit is said to be operating in *continuous* mode. On the other hand, if the inductance is too small or the switching period is relatively too long, the inductance current may drop to zero before the next period begins, introducing an "idling" interval during which both diode D and switch S are not conducting. This mode of operation is referred to as *discontinuous* mode. When operating in discontinuous mode, the circuit toggles between three linear networks corresponding to three different switch states, as depicted in Table I. In continuous mode, the third state is omitted, and $t_n'' = t_{n+1}$.

The boost converter operating in discontinuous mode can thus be described by the following sequence of state equations:

$$\begin{aligned} \dot{x} &= A_1 x + B_1 E \quad && t_n \le t < t_n' \\ \dot{x} &= A_2 x + B_2 E \quad && t_n' \le t < t_n'' \\ \dot{x} &= A_3 x + B_3 E \quad && t_n'' \le t < t_{n+1} \end{aligned} \tag{2}$$

TABLE I.
SWITCH STATES

Interval	Switch S	Diode D
$t_n \le t < t'_n$	Closed	Open
$t'_n \le t < t''_n$	Open	Closed
$t''_n \le t < t_{n+1}$	Open	Open

where x is the state vector $[v_c \;\; i_L]^T$, E is the input voltage, the A's and B's are given by

$$A_1 = \frac{1}{C(R+r_c)}\begin{bmatrix} -1 & 0 \\ 0 & 0 \end{bmatrix}, \quad B_1 = \begin{bmatrix} 0 \\ \frac{1}{L} \end{bmatrix} \tag{3}$$

$$A_2 = \frac{1}{C(R+r_c)}\begin{bmatrix} -1 & R \\ \frac{-CR}{L} & \frac{-CRr_c}{L} \end{bmatrix}, \quad B_2 = \begin{bmatrix} 0 \\ \frac{1}{L} \end{bmatrix} \tag{4}$$

$$A_3 = \frac{1}{C(R+r_c)}\begin{bmatrix} -1 & 0 \\ 0 & 0 \end{bmatrix}, \quad B_3 = \begin{bmatrix} 0 \\ 0 \end{bmatrix} \tag{5}$$

Two points are worth noting here. First, the value of the inductance must be sufficiently small to ensure that the circuit operates in discontinuous mode. It can be shown that the inductance L must not exceed $D(1-D)^2RT/2$ for a discontinuous-mode operation [6], where D is the duty cycle and T is the switching period. Second, since the solution to each of (2) can be expressed explicitly in terms of the respective transition matrix, simulation of cycle-by-cyle time-domain waveforms is possible using the above piecewise switched model. We shall base all our simulations on this model.

III. Derivation Of The Poincaré Map

Although the piecewise switched model described in the foregoing section is undeniably the most accurate description of the actual circuit operation, it does not allow analysis to be performed in a convenient fashion. As the system is periodically driven, it is possible and desirable to represent it by an iterative map in which the value of x at $t = nT$ is expressed in terms of that at $t = (n-1)T$, where T is the period of the switching cycle. As is well known in the literature of chaos, such a map will also facilitate the investigation of subharmonics and chaos [7].

3.1 Order of the System

Before embarking on the derivation of the iterative map, we must note that although the equivalent networks corresponding to all switch states are second order linear networks, the inductance current i_L does not really act as a state variable. This is because, in the discontinuous mode of operation, the inductance current always drops to zero during the interval when both switch S and diode D are not conducting. In other words, $i_L = 0$ for all $t = t_n = nT$. Thus the system is first order, and can be described by a first-order map.

3.2 Derivation of Poincaré Map by Successive Substitution

As shown in Section 2, there are three constituent topologies, each of which is represented by a state equation, and the solution to each state equation can be explicitly determined. For example, the solution in the interval $t_n < t < t'_n$ is given by

$$x(t) = \Phi_1(t-t_n)x(t_n) + \int_{t_n}^{t} \Phi_1(t-\tau)B_1E.d\tau \tag{6}$$

$$= \Phi_1(t-t_n)\left(x(t_n) + \int_{t_n}^{t} \Phi_1(t_n-\tau)B_1E.d\tau\right). \tag{7}$$

Thus, "stacking" consecutive solutions over a switching period would result in an iterative map that expresses $x(t_{n+1})$ in terms of $x(t_n)$, i.e.,

$$\begin{aligned} x(t_{n+1}) =& \Phi_3(t_e)\Phi_2(t_d)\Phi_1(t_c) \\ & \cdot \left(x(t_n) + \int_{t_n}^{t'_n} \Phi_1(t_n-\tau)B_1E.d\tau\right) \\ & + \Phi_3(t_e)\Phi_2(t_d)\int_{t'_n}^{t''_n} \Phi_2(t'_n-\tau)B_2E.d\tau \\ & + \Phi_3(t_e)\int_{t''_n}^{t_{n+1}} \Phi_3(t''_n-\tau)B_3E.d\tau \end{aligned} \tag{8}$$

where $t_c = t'_n - t_n$, $t_d = t''_n - t'_n$, $t_e = t_{n+1} - t''_n$, and the transition matrix $\Phi_k(\xi)$ is given by the following series:

$$\Phi_k(\xi) = \mathbf{1} + \sum_{n=1}^{\infty} \frac{1}{n!}A_k^n\xi^n \quad \text{for } k = 1, 2, 3. \tag{9}$$

When all transition matrices have been computed and substituted in (8), an iterative map results:

$$x(t_{n+1}) = f(x(t_n), d_n) \tag{10}$$

where d_n is the duty cycle during the nth period, defined as

$$d_n = \frac{t_c}{T}. \tag{11}$$

Looking at the form of (10), it is clear that d_n is an input variable which can be varied to regulate the system. In practice, the value of d_n is adjusted via a *pulse-width modulator*, which turns on switch S at $t = nT$ for a duration of d_nT. When d_n is assigned to a fixed value, the system is said to be uncontrolled or *open loop*. On the other hand, when d_n is varied according to x, the system is said to be a *closed-loop* system.

As mentioned previously, (10) is essentially a first-order map, since $i_L(t_n) = 0$ for all n. In the sequel, x will be used to denote only the capacitance voltage v_c.

3.3 Finite Series Approximation

In typical applications of switching regulators, the switching period is much shorter than the capacitance-load-resistance time constant. This condition greatly simplifies the evaluation of the transition matrix $\Phi_k(.)$ [6], and results in a very accurate approximation of $\Phi_k(.)$ as a finite series

$$\Phi_k(\xi) = \mathbf{1} + A_k\xi + \frac{1}{2}A_k^2\xi^2 \quad \text{for } k = 1, 2, 3. \tag{12}$$

Furthermore, during the interval $t_n < t < t'_n$, the inductance current i_L increases linearly from zero to a value i_{max} at a rate of E/L, and during $t'_n < t < t''_n$, it decreases linearly from i_{max} to zero at a rate of $(x - E)/L$. Thus we can write

$$\frac{t_d}{t_c} = \frac{E}{x - E}. \tag{13}$$

Using (3)–(5), (12), and (13), and knowing that $i_L(t_n) = 0$ for all n, (8) can be approximated as

$$x_{n+1} = \alpha x_n + \frac{\beta d_n^2 E^2}{x_n - E} \tag{14}$$

where

$$x_n = v_c(t_n) = v_c(nT) \tag{15}$$

$$\alpha = 1 - \frac{T}{C(R + r_c)} + \frac{T^2}{2C^2(R + r_c)^2} \tag{16}$$

and

$$\beta = \frac{RT^2}{2LC(R + r_c)}. \tag{17}$$

Remarks: The map represented by (14) generates values of x at $t = nT$ for all positive integer n. Obviously, the usefulness of this map lies in its ability to predict the flow of the system. In particular, if the system is a contraction, i.e., $\|f(x) - f(x')\| < \|x - x'\|$ for all x and x', it is guaranteed to converge to a unique fixed point. In fact, it has been shown [8] that (8) is a contraction for all d, and hence the open-loop system has a unique fixed point for all d. However, (14) is clearly not contracting when $(x-E)$ is sufficiently small, since we can find some d for which $\|f(x) - f(x')\| \geq \|x - x'\|$ for some x and x'. Such discrepancy is due to the approximation introduced in (12), which causes (14) to deviate from (8) at some value of d when $(x-E)$ is small. Fortunately, we will not use (14) to study the system under such conditions. Detailed discussions of this issue are given in [6], and will not be pursued in this paper.

3.4 Approximate Poincaré Map for the Closed-Loop System

Our attention here is focused on the system controlled by the following simple feedback scheme:

$$\Delta d_n = -\kappa . \Delta x_n \tag{18}$$

where κ is the feedback factor and can be chosen to modify the closed-loop dynamics. Fig. 2 shows the schematic diagram of the closed-loop system. Note that the above equation implies the use of a uniform sampling scheme in which the value of $\Delta x(t_n)$, sampled and held at the start of every switching period, is used to derive Δd for that switching period.

The Poincaré map for the closed-loop system can now be derived by putting (18) in (14), giving

$$x_{n+1} = \alpha x_n + \frac{h(d_n)^2 \beta E^2}{x_n - E} \tag{19}$$

where

$$d_n = D - \kappa(x_n - X) \tag{20}$$

$$h(d_n) = \begin{cases} 0 & \text{if } d_n < 0 \\ 1 & \text{if } d_n > 1 \\ d_n & \text{otherwise.} \end{cases} \tag{21}$$

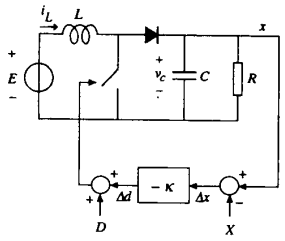

Fig. 2. Schematic diagram of the closed-loop system.

Note that the uppercase letter denotes the steady-state (desired) value of the variable concerned, and that $h(.)$ represents the inherent *saturating nonlinearity* of the pulse-width modulator. As the system is open-loop stable, D can be uniquely determined by putting $x_{n+1} = x_n = X$ in (14), i.e.,

$$D = \sqrt{\frac{(1 - \alpha)(X - E)X}{\beta E^2}}. \tag{22}$$

It will be shown later on in this paper that (19) represents a typical *unimodal* map [7], i.e., one that has one local minimum or maximum, which is well known to exhibit a period-doubling route to chaos.

IV. Stability and the Characteristic Multiplier

In the design of any closed-loop system, the most fundamental requirement is stability. In simple words, the system should be designed in such a way that any disturbance superposed onto the steady-state fixed point will diminish and eventually reduce to zero. A usual way to determine the stability of a fixed point X is to consider the Taylor series expansion of Δx_{n+1} around the fixed point

$$\Delta x_{n+1} = \sum_{k=1}^{\infty} \frac{1}{k!} \frac{\partial^k f(x)}{\partial x^k}\bigg|_{x=X} (\Delta x_n)^k \tag{23}$$

where $\Delta x_n = x_n - X$. Thus, if the disturbance is small, the magnitude of $\partial f(x)/\partial x$ at $x = X$ determines the stability. This partial derivative will be referred to, in the sequel, as the *characteristic multiplier* at the fixed point X, and will be denoted by λ.

To simplify our analysis, we assume that the steady-state value of d_n falls in the range $0 < d_n < 1$. Thus, in the neighborhood of the steady-state point, we may ignore the effect of saturating nonlinearity. In the case of the simple feedback scheme represented by (18), a stable closed-loop system can be achieved by assigning an appropriate value to κ so that the magnitude of the characteristic multiplier, λ, is less than one, i.e.

$$-1 < \alpha - \frac{\beta D^2 E^2}{(X - E)^2} - \frac{2\beta D E^2 \kappa}{X - E} < 1. \tag{24}$$

V. Flip Bifurcations and Subharmonics

Crossing the boundary of the stable region, the system bifurcates into a new regime of dynamical behavior. In this section, we focus on the bifurcation at $\lambda = -1$. Clearly, when $\lambda = -1$,

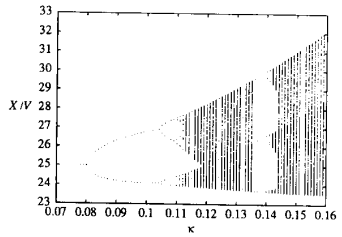

Fig. 3. Bifurcation diagram using the approximate Poincaré map.

x repeats itself every second period, and as λ decreases further, x may either diverge in an oscillatory fashion or maintain a stable subharmonic oscillation, depending upon the higher-order terms in (23). The critical value of the feedback factor corresponding to $\lambda = -1$ can be found from (24) as

$$\kappa_c = \left(1 + \alpha - \frac{\beta D^2 E^2}{(X-E)^2}\right)\frac{X-E}{2\beta D E^2}. \tag{25}$$

Using (19) to (21), we can easily arrive at some useful conclusion concerning the behavior of the system near $\kappa = \kappa_c$. As mentioned before, (19) represents a typical unimodal map. A common plan of attack for such maps is as follows. Initially we set κ at a value smaller than κ_c and confirm that the system has a stable fixed point. Then, we increase κ and observe the way the system loses stability and bifurcates into subharmonic orbits of period two. We further increase κ to observe a typical subharmonic cascade and eventually chaotic motion.

An example will help visualize the situation. Suppose $T/C(R+r_c) = 0.12$, $RT/L = 20$, $E = 16V$, and $X = 25V$. This gives $D = 0.2874$. Also it is readily verified that the value of RT/L is large enough to ensure a discontinuous-mode operation. Thus, using (19)–(21), the system under the control of (18) is represented by

$$x_{n+1} = 0.8872x_n + \frac{1.2 \times 16^2 \times h(d_n)^2}{x_n - 16} \tag{26}$$

where $d_n = 0.2874 - \kappa(x_n - 25)$. The characteristic multiplier, as given in (24), is

$$\lambda = 0.5739 - 19.6198\kappa. \tag{27}$$

Thus the critical value of κ is 0.08. Using (26), a bifurcation diagram can be generated as shown in Fig. 3. Reference to this diagram shows that the system becomes chaotic when κ is larger than about 0.111.

It must be emphasized that the foregoing analysis has been based on the approximate Poincaré map given by (26). In Section 6, we will simulate the system using the exact piecewise switched model described in Section 2 and confirm the kind of behavior predicted above.

VI. Computer Simulation of Subharmonics and Chaos

At switching frequencies as low as 3 kHz, parasitic effects can be safely neglected, and the piecewise switched model represents a very accurate description of the system. We have written a computer program, based on this model, for simulating the boost converter controlled by the simple feedback law of (18). The values of the circuit parameters used in the simulation are consistent with the example given in the previous section, as summarized in Table II. For the sake of consistency with the foregoing theoretical discussion, a uniform sampling scheme is employed in the proportional feedback in our simulation, i.e., values of x are sampled and held at $t = nT$.

TABLE II.
Simulation Parameters

Circuit Parameters	Values
Switching period T	333.33μsec
Input voltage E	16V
Output voltage X	25V
Power	50W
Inductance L	208μH
Capacitance C	222μF
Load resistance R	12.5Ω (consistent with power)

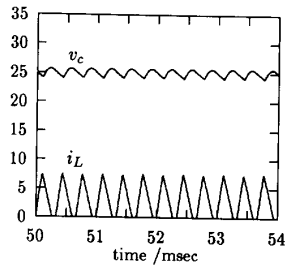

Fig. 4. Fundamental waveforms from simulation of the exact state equation with $\kappa = 0.07$.

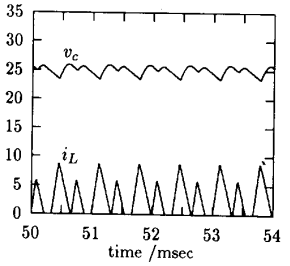

Fig. 5. Period 2 subharmonic waveforms from simulation of the exact state equation with $\kappa = 0.097$.

We have simulated the steady-state waveforms for various values of κ belonging to subcritical ($\kappa < \kappa_c = 0.08$) and supercritical ($\kappa > \kappa_c = 0.08$) cases. Figs. 4–7 show the steady-state waveforms of the closed-loop system with $\kappa = 0.07$, 0.097, 0.107, and 0.14, respectively. The phase portraits corresponding to these four cases are shown in Figs. 8–11, which demonstrate clearly the fundamental, period-2 subharmonic, period-4 subharmonic, and chaotic orbits. We have also summarized in Fig. 12 the steady-state information in the form of a bifurcation diagram that demonstrates clearly the sequence of period-doubling subharmonics, as well as the presence of a period-3 window around $\kappa = 0.165$.

The general appearance of this simulation-based bifurcation diagram resembles that of Fig. 3. However, some noticeable differences are still observed between them, which may be explained as follows:

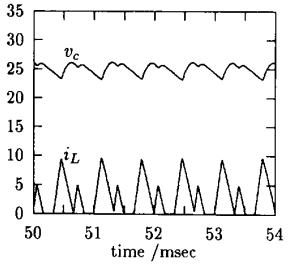

Fig. 6. Period 4 subharmonic waveforms from simulation of the exact state equation with $\kappa = 0.107$.

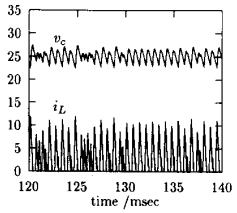

Fig. 7. Chaotic waveforms from simulation of the exact state equation with $\kappa = 0.14$.

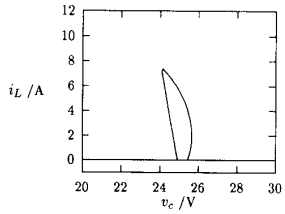

Fig. 8. Phase portrait of a fundamental orbit from simulation of the exact state equation with $\kappa = 0.07$.

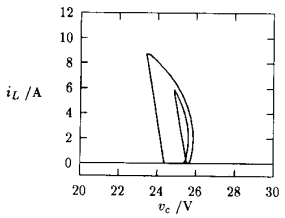

Fig. 9. Phase portrait of a period 2 subharmonic orbit from simulation of the exact state equation with $\kappa = 0.097$.

1) Fig. 3 is generated from an approximate iterative map whose validity relies very much on the accuracy of the truncated Taylor series, namely, (12). On the other hand, Fig. 12 represents exact system behavior.
2) In the derivation of the approximate iterative map we have assumed that the system is composed of three switch states for every period, i.e., the converter being operated *generically* in the discontinuous mode. However, as clearly seen from our simulated waveforms, the system occasionally enters into continuous mode where only two switch states are manifested. This phenomenon is readily observable when the system is exhibiting subharmonic or chaotic motion.

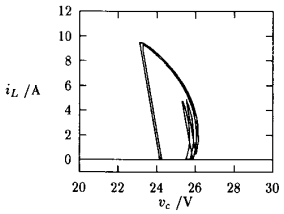

Fig. 10. Phase portrait of a period 4 subharmonic orbit from simulation of the exact state equation with $\kappa = 0.107$.

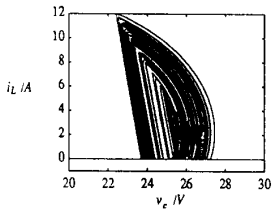

Fig. 11. Phase portrait of chaotic orbit from simulation of the exact state equation with $\kappa = 0.14$.

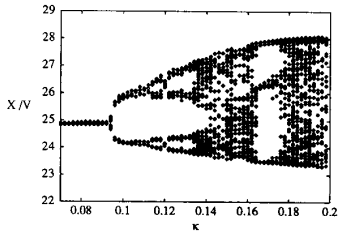

Fig. 12. Bifurcation diagram from computer simulation; 500 consecutive $x(nT)$ after transient are plotted for each κ.

The second point illustrates an important structural property of the switching regulator that constitutes a unique feature of the chaotic attractor for this type of circuits. As will be further substantiated in the next section, chaos occurs when the circuit randomly enters into continuous mode of operation while its dominating operating mode is still the discontinuous mode.

VII. Experimental Verification

In Section 5, a period-doubling subharmonic cascade was predicted on the basis of an approximate Poincaré map, and in Section 6, we simulated the exact circuit and witnessed the presence of chaotic motion. Without doubt, it would be even more convincing if chaos is actually observed in real circuits.

7.1 The Experimental Circuit

Fig. 13 shows the schematic of our experimental boost switching regulator. The switch is implemented by a MOSFET whose on-off status is controlled by a pulse-width modulated signal. The switch is *on* when the positive input of the comparator is larger than the saw-tooth voltage, and is *off* otherwise. Thus, the duty cycle is determined by the control voltage v_{con}. The small-signal relation between v_{con} and the

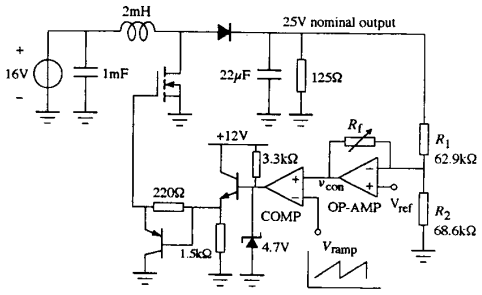

Fig. 13. Schematic of the experimental boost regulator.

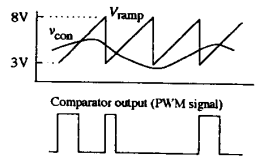

Fig. 14. Pulse-width modulation.

duty cycle is given by

$$\Delta v_{\text{con}} = V_M \Delta d \tag{28}$$

where V_M is the height of the sawtooth voltage. Fig. 14 depicts this situation. The loop is closed by connecting the op-amp input to the converter output via a resistor ladder R_1–R_2, as shown in Fig. 13. Assuming an ideal op-amp characteristic, the following equation relating v_{con} and x is immediately clear:

$$v_{\text{con}} = \left(1 + \frac{R_f}{R_1 \parallel R_2}\right) V_{\text{ref}} - \frac{R_f}{R_1} x. \tag{29}$$

Separating the small-signal variation from the steady-state condition yields

$$\Delta v_{\text{con}} = -\frac{R_f}{R_1} \Delta x. \tag{30}$$

From (29) and (28), we have

$$\Delta d = -\frac{R_f}{V_M R_1} \Delta x. \tag{31}$$

Comparing (31) with the feedback equation, namely (18), we immediately see that the feedback factor κ can be adjusted by varying R_1 and R_f, since

$$\kappa = \frac{R_f}{V_M R_1}. \tag{32}$$

Furthermore, the desired steady-state condition can be achieved by choosing a correct value for V_{ref}.

Remarks: In our theoretical and simulation studies, we have employed a uniform sampling scheme for the feedback control. In our experiments, however, natural sampling is used for the sake of simplicity, as shown in Fig. 14. Thus, (18) and (31) are not actually equivalent. This inevitably introduces a subtle source of error if κ is adjusted according to (32). Nevertheless, such discrepancy in the sampling scheme has little effect on our result concerning the period-doubling route to chaos, as will be verified in the following subsections.

Fig. 15. Period 2 subharmonic waveforms from experimental circuit with $\kappa \approx 0.09$.

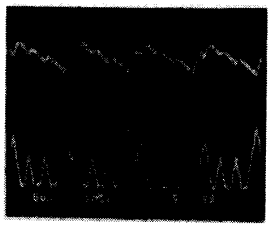

Fig. 16. Period 4 subharmonic waveforms from experimental circuit with $\kappa \approx 0.12$.

Fig. 17. Phase portrait of period 2 subharmonic motion from experimental circuit with $\kappa \approx 0.09$.

7.2 Circuit Parameters and Results

In our experiment we have deliberately lowered the power level to 5W so as to minimize device stress. Thus, the load resistance is 125Ω. The switching frequency is 3kHz which is low enough to ensure that the circuit is unaffected by high-frequency problems. The values of RT/L and T/CR are chosen to align with those used in our simulation studies. Figs. 15 and 16 show typical period-2 and period-4 subharmonic waveforms, respectively. Oscilloscope pictures of the phase portraits corresponding to these two cases are shown in figures 17 and 18. To obtain the chaotic waveform and corresponding phase portrait, a digital storage oscilloscope is employed. Steady-state waveforms are captured over a sufficiently long interval and are shown in Figs. 19 and 20.

7.3 Saturation and Switching Patterns

Our experiments have also confirmed one important feature of the dynamics exhibited by this type of systems. The toggling between discontinuous mode (three state) and continuous mode (two state) is clearly noticeable when the system is exhibiting subharmonic or chaotic motion. For example, in Fig. 16, one two-state period and three three-state periods repeat themselves to produce a period-4 subharmonic waveform. For

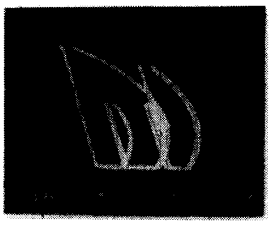

Fig. 18. Phase portrait of period 4 subharmonic motion from experimental circuit with $\kappa \approx 0.12$.

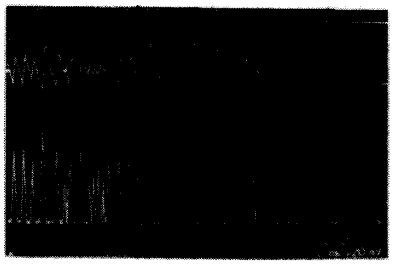

Fig. 19. Chaotic waveforms from experimental circuit with $\kappa \approx 0.15$.

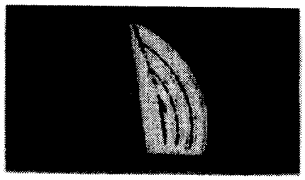

Fig. 20. Phase portrait of chaotic motion from experimental circuit with $\kappa \approx 0.15$.

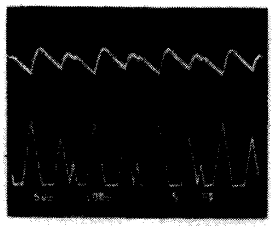

Fig. 21. Period 4 subharmonic waveform from experimental circuit showing skipped cycles.

Fig. 22. Phase portrait of period 4 subharmonic motion from experimental circuit showing skipped cycles.

simplicity, we say that this particular subharmonic motion has a '2-3-3-3' pattern in which the integer number indicates the number of switch states that have been involved in a period.

To make things worse, *saturating nonlinearity* of the pulse-width modulator may come into play under certain conditions. As modeled by the function $h(d)$ introduced earlier in Section 3.4, saturating nonlinearity effectively confines the value of d within the range $0 \leq d \leq 1$. For the system to be Lagrange stable (i.e. bounded), the upper limit should never be reached. This is because once switch S is turned on for the entire period, the output voltage decreases monotonically, and the feedback forces $d = 1$ for all subsequent periods. The inductance current thus rises toward infinity. In our experiments, such a catastrophic operation has been carefully avoided by selecting a relatively small steady-state duty cycle and letting the circuit start at a reasonably high initial output voltage. Thus, the duty cycle has always been kept strictly below one. On the other hand, periods with zero duty cycle can be allowed. In fact, it has been repeatedly observed in our experimental circuit that "blank" periods are present for some values of κ, as exemplified in Figs. 21 and 22 where the period-4 subharmonic waveform has a '2-1-2-3' pattern, in which '1' means a "blank" period or a skipped cycle. Detailed inspection of the circuit and waveforms reveals that, in the period preceding the "blank" period, the circuit operates in continuous mode and a very high output voltage occurs, causing the value of v_{con} to drop below the lower threshold of V_{ramp}, as illustrated in Fig. 14. The switch is thus open for the entire "blank" period, and the inductance current simply drops to zero and remains at zero for the rest of that period. It should be noted that the phase portrait shown in Fig. 22 looks deceptively like a period-3 orbit, and is actually a period-4 orbit with one loop shrunk to zero area.

In the chaotic region, no fixed patterns can be identified, and the steady-state behavior may be vaguely related to a "random" selection of switching patterns from either two-state, three-state, or "blank" periods. It may be conceived that a special kind of randomness, arising from the ability of the system to change its configuration in more than one pre-defined patterns, constitutes a unique feature of the chaotic dynamics of switched-mode converter circuits.

VIII. Conclusions

Circuits containing pulse-width modulators are potentially chaotic systems. Although theoretical studies of chaos in PWM systems appeared as early as in 1980 [9],[10], experimental verifications have rarely been reported. An objective of this paper is to demonstrate the possibility of a chaotic dynamical regime in a very common PWM switching regulator. We have shown theoretically, by simulation, and experimentally, that a simple boost regulator operating in discontinuous mode can easily become chaotic. When the system is exhibiting chaos, its order shuffles randomly between one and two. Such structural instability represents a rather unique feature of the chaotic motion exhibited by switching converter circuits. It can be anticipated that many interesting chaotic attractors would show up in higher-order converter circuits. From a more general perspective, the class of multistructural system, which covers the whole of power electronics circuits, is as easily attracted to chaos as the many previously studied chaotic circuits [5].

ACKNOWLEDGMENT

The author wishes to thank Chan Wing for his able assistance in constructing the circuits used in the experiment.

REFERENCES

[1] J.H.B. Deane and D. C. Hamill, "Instability, subharmonics and chaos in power electronic systems," *IEEE Trans. Power Electron.*, vol. 5, no. 3, pp. 260–268, 1990.
[2] D. C. Hamill, J.H.B. Deane, and D. J. Jefferies, "Modeling of chaotic dc-dc converters by iterative nonlinear mappings," *IEEE Trans. Power Electron.* vol. 7, no. 1, pp. 25–36, 1992.
[3] H. Bai-Lin, Ed., *Chaos.* Singapore: World Scientific, 1984.
[4] A. V. Holden, Ed., *Chaos.* Princeton, NJ: Princeton University Press, 1986.
[5] L. O. Chua, Ed., *Special Issue on Chaotic Syst., Proc. IEEE,* vol. 75, no. 8, pp. 979–1120, 1987.
[6] C. K. Tse and K. M. Adams, "Qualitative analysis and control of a dc-dc boost converter operating in discontinuous mode," *IEEE Trans. Power Electron.*, vol. 5, no. 3, pp. 323–330, 1990.
[7] J.M.T. Thompson and H. B. Stewart, *Nonlinear Dynamics and Chaos.* Chichister, England: Wiley, 1988.
[8] C. K. Tse and K. M. Adams, "On the steady state analysis of switched mode power converters," *Int. J. Circ. Theory Appl.*, vol. 20, no. 1, pp. 99–105, 1992.
[9] J. Baillieul, R. W. Brockett, and R. B. Washburn, "Chaotic motion in nonlinear feedback systems," *IEEE Trans. Circ. Syst.*, vol. CAS-27, no. 11, pp. 990–997, 1980.
[10] D. Veitch, "Windows of stability in control chaos," *IEEE Trans. Circ. Syst.*, vol. 39, no. 10, pp. 808–819, 1993.

Chi K. Tse (M'90) received the B.Eng. (Hons) and Ph.D. degrees from the University of Melbourne, Australia, in 1988 and 1991, respectively.

He has worked in software development with an Australian database company for some years. He also spent a short period of time with Astec International Limited as a senior engineer responsible for the design of commercial power supplies. He is presently a lecturer in the department of electronic engineering at Hong Kong Polytechnic where his interests are in circuit theory and power electronics.

Dr. Tse was awarded the L. R. East Prize by the Institution of Engineers, Australia, in 1988.